

# Earth Observation and Geomatics Engineering

Homepage: https://eoge.ut.ac.ir/

#### Online ISSN: 2588-4360

# Reconstruction of 3D Building Edges to Improve DSM Generated from UAV Multi-Images

Abire Bazyar<sup>1</sup> (in), Marzieh Jafari<sup>2</sup> (in) and Hadiseh Hasani<sup>3⊠</sup> (in)

- 1. Department of Geodesy and Surveying Engineering, Tafresh University, Tafresh 3951879611, Iran. E-mail: babireh5@gmail.com
- 2. Department of Geodesy and Surveying Engineering, Tafresh University, Tafresh 3951879611, Iran. E-mail: jafaro@tafreshu.ac.ir
- 3. Corresponding author, Department of Geodesy and Surveying Engineering, Tafresh University, Tafresh 3951879611, Iran. E-mail: h.hasani@tafreshu.ac.ir

# Article Info ABSTRACT

Article type: Research Article

#### Article history:

Received 2025-02-19 Received in revised form 2025-06-01 Accepted 2025-06-08 Published online 2025-10-19

#### Keywords:

Digital Surface Model (DSM), 3D Line Reconstruction, Least Squares, Point Cloud, Building Edge Digital surface model (DSM) generation of urban scenes encounters some challenges, especially for man-made feature boundaries with high altitudes. It leads to the saw-tooth effects at the features edges in the orthophoto images. To mitigate these artifacts, this study proposes a novel methodology employing three-dimensional (3D) line segment extraction, enabling precise reconstruction of building edges in three-dimensional space.

Firstly, the relevant 2D lines from multi-images are extracted then these segments reconstruct the 3D line segments by intersecting multiple planes, estimating the optimum intersection parameters of the line based on the least squares methodology, and applying restrictions at the end point of the line. Finally, the 3D line segments are divided into discrete 3D points to be included in the 3D point clouds. After the classification of points on both sides of the line and masking points around the line between the inner and outer edges as the parapet wall of the roof, the height of the nearest line point is assigned to all points within the mask.

Regarding the numerical results, 99% improvement in height point cloud consistency was attained through advanced masking techniques. As a result, a more complete and accurate TIN can be developed to provide important essential data for products such as DSM and orthophoto.

Experimental results of this approach show that saw-tooth effects at the edges of the building can be greatly improved; so, the quality of DSM and orthophoto increases significantly.

Cite this article: Bazyar, A., Jafari, M., & Hasani, H. (2025). Reconstruction of 3D building edges to improve DSM generated from UAV multi-images, Earth Observation and Geomatics Engineering, Volume 8, Issue 2, Pages 9-23. http://doi.org/10.22059/eoge.2025.390296.1168



© The Author(s).
DOI: http://doi.org/10.22059/eoge.2025.390296.1168

Publisher: University of Tehran.

#### 1. Introduction

In recent years, UAV photogrammetry has become an efficient tool in a wide range of applications such as urban 3D modelling and mapping due to its low cost and high flexibility in 3D point cloud generation (Jiménez-Jiménez et al., 2021). The general process of producing a 3D model is to take overlapped images of the object/region, aerial triangulation, produce epipolar images, dense matching, and finally point cloud of the object/region generation (Nex & Remondino, 2014). However, DSM obtained from aerial images has low quality at the man-made boundaries, due to the edge blurring, dislocation, altitude variation on both sides, and saw-tooth (Wang et al., 2018).

Dense matching is the key step to generate 3D model and several algorithms are proposed for this purpose, which are generally divided into three categories: local, global and semi-global matching algorithms (Dall'Asta & Roncella, 2014). Local methods use the neighborhood information of each pixel to determine the corresponding point in another image. These algorithms are sensitive to ambiguous local areas in images (such as occlusions and poorly textured areas). Global methods are based on minimizing the energy function and are more robust for ambiguous local areas, but require considerable computation. To overcome the limitations of global and local methods, advances have been made that aim to take advantage of both methods. The Semi-Global Matching (SGM) algorithm is one of the most advanced algorithms developed in this field, which is widely used for commercial and applied software (Lu et al., 2021).

The SGM algorithm has been used in various applications. This method provides an efficient relationship between execution time and accuracy, especially at object boundaries and delicate structures. It is also stable to radiometric differences and has less sensitivity to the choice of parameters; therefore, it is suitable for solving practical problems (Ma et al., 2022). Despite advances of the SGM, there are usually still some mismatches and outliers. Moreover, it faces challenges in urban areas such as complexity, variety, objects proximity (buildings and vegetation), and occlusions. Consequently, in DSM, the edges are still not modelled properly and are not accurate enough (Wu, 2021). Accordingly, the orthophoto result is not produced with acceptable accuracy, especially at building boundaries (Chen et al., 2021).

Edges, as one of the most important features of manmade objects often not created accurately with dense matching. Due to the lack or absence of points on the edges in the image, it appears the saw-tooth effect. Since edges are key components in the reconstruction and mapping of features (e.g. building), increasing the accuracy of edge reconstruction in the DSM improves the accuracy of object reconstruction; therefore, edge quality improvement algorithms in the DSM are of great importance (Wang et al., 2018).

According to the availability and cost effectiveness of UAV image, several researches have been performed to evaluate the potential of these images in DSM generation (Bhandari et al., 2015; Qin et al., 2021). To improve DSM, two solutions can be mentioned: 1) select an appropriate method to generate dense and accurate point cloud, 2) using algorithms to improve the derived point cloud and also eliminate outliers.

Liu et al. (2015) proposed an automatic large-scale 3D reconstruction based on low-altitude UAV images. Dense point clouds are generated by feature extraction, image matching, structure from motion (SfM) and multi-view stereo (MVS) algorithms. In this approach without the requirement of previous camera calibration or any other external prior knowledge, the running time of feature matching for large scene reconstruction is reduced by taking advantage of the flight-control data from UAV., to reduce (Liu et al., 2015). A multi-view stereo algorithm for generating a denser point cloud based on low-altitude remote sensing images was proposed by Shao et al. (2016). They employed a patch-based Multi-photo Geometrically Constrained Matching (MPGC) on the expanded patch for each point to optimize points based on constrained least square adjustment with the space geometry relationship, and epipolar line (Shao et al., 2016).

A powerful image matching algorithm must be able to extract a dense 3D point cloud with sufficient resolution to describe the surface of objects and their discontinuities. Therefore, the point density must be adjusted to preserve the edges. But 3D reconstruction in urban areas is difficult due to the complexity of the scene, and the resulting boundaries are often poorly contrasted. As a result, the detectors lose the boundary lines, and only a complete 3D reconstruction should be done. The researches that solve this problem are based on extracting and matching edges.

Su et al. (2018) proposed an edge constraint and outline compensation (ECAOC) dense matching method to preserve the structural features of the building in the disparity map. The improved edge lines are used to optimize the matching search scope and matching template window. Highprecision building edges are used to compensate the building shape features (Su et al., 2018). Chuang et al. (2018) present a gradual SGM cost aggregation algorithm that includes a penalty tuning process and edge feature knowledge. They propose a penalty parameter and a weighting process to consider edge pixels with depth variations, to obtain satisfactory depth estimation by preserving sharp edges and smoothness without noise (Chuang et al., 2018). In this year, Yue et al. (2018) proposed the combination of Canny detection algorithm and CSCA (Cross-scale Cost Aggregation) algorithm to calculate the disparity map and its error rate which could eliminate a lot of inappropriate information and reduce the

time of data processing also improve the accuracy of disparity map (Yue et al., 2018). Liu et al. (2023) applied a deep learning (DL) based framework for 3D reconstruction of oblique images. For this purpose, aerial triangulation is performed, and then DL model is implemented to generate depth map from images. Finally, they are fused and a textured point cloud is generated (Liu et al., 2023).

Although development in matching algorithms, increase reliability of the point cloud generation, but there are still some areas which cannot be matched and a small number of outliers exist. Another approach to improve the DSM is to extract and match additional information from images and integrate with the final point cloud. Finally, the 3D surface is reconstructed using interpolation methods.

In 2002, McIntosh and Krupnik corrected the DSMderived laser scanner, using photogrammetric data. The edges are extracted from stereo images, and they were matched by feature-based matching techniques. Then, a 3D reconstruction of the corresponding edges is performed. These edges are used to obtain precise locations of surface discontinuities in the urban scene (McIntosh & Krupnik, 2002). Bignoli et al. (2018) proposed a framework to reconstruct straight and curved edges to enhance the recovered surface. For this purpose, a graph-based representation of 2D edges in images is applied (Bignoli et al., 2018). In 2018, Wang et al. (2018) proposed a method aimed at removing the saw-tooth effects on the edges by accurately 3D building edges reconstruction. First 2D line segments are first extracted and matched by a pair of images, then by joining two planes 3D line segments are reconstructed of constrained to the line end-points. To construct a more accurate triangulated irregular network (TIN) model for true orthophoto production, the line segments are integrated into the obtained discrete 3D point cloud. The experimental results of this study show that the saw-tooth effects can be removed, which leads to a significant improvement in quality in real orthophoto (Wang et al., 2018).

DL is another solution to reconstruct 3D building models which attract some attentions during last years. Alidoost et al. (2019) reconstructed 3D model from single 2D image based on convolutional neural network (CNN). Building detection and refinement is implemented in two-stage network (Alidoost et al., 2019). Ebrahimikia and Hosseininaveh (2022) applied DL to structural building edges and improve 3d point cloud by adding 3D edge points. The results are obtained on aerial image and prove the accuracy of the proposed method (Ebrahimikia & Hosseininaveh, 2022).

To solve the problems of saw-tooth effects and distortion at the edges, so far solutions have been developed by combining computer vision science techniques and matching algorithms to produce DSM and orthophoto with high resolution. In this regard, this paper intends to present an algorithm for UAV multi-image of a scene. In previous

studies, just two images were considered, but each building boundary has usually been captured in more images. Therefore, the proposed method uses multi-image bundle adjustment method to accurately reconstruct 3D building edges. In the case of multi-images, the 3D line is extracted from the intersection of multi-plane. Because the intersection of all planes is not a single line, the optimum line direction is estimated from the intersection of planes in pairs using the least squares method. The 3D line segments are integrated into the obtained point cloud. Following the classification of point clouds into roof and ground points, the roof point cloud is refined by first masking points along the parapet wall boundary between inner and outer edges. The mask width has been set approximately equal to the parapet wall thickness. Second, the average height of the points inside the mask is assigned to all masked point clouds. DSM and orthophoto are produced based on the final point cloud.

This paper consists of 4 sections. First, an introduction and literature review on the importance and necessity of DSM improvement and research objectives were presented. Section 2 describes the proposed method to improve the DSM obtained from UAV images by removing the saweffects on the edges, using the corresponding 3D line segmentation. In section 3 the results obtained from the proposed method on the UAV images are presented. Finally, conclusions and suggestions are included in the last section.

# 2. Methodology

The proposed method to solve the problems of saw-tooth effects and improve the DSM based on the generation of 3D lines corresponding to edges using the multi-image bundle adjustment method is algorithmically presented in the flowchart (Figure 1).

The descriptions of this algorithm in details are presented as follows:

- 1) Use existing photogrammetric algorithms and software to generate point cloud and preprocessing for outlier detection and denoising to simplify the generated point cloud.
- 2) Extraction of 3D lines related to the building edges using the multi-image bundle adjustment method, generate end points and their discretization.
- 3) Edge point clouds Refinement
- 4) Refinement the final point cloud for surface reconstruction using interpolation methods and saw-tooth effects to achieve a more accurate DSM and orthophoto.

# 2.1. Point cloud generation and pre-processing

In order to produce DSM, dense point cloud must be created which usually contains blunders and noisy points due to mismatching. consequently, preprocessing is required to improve 3D point cloud quality.

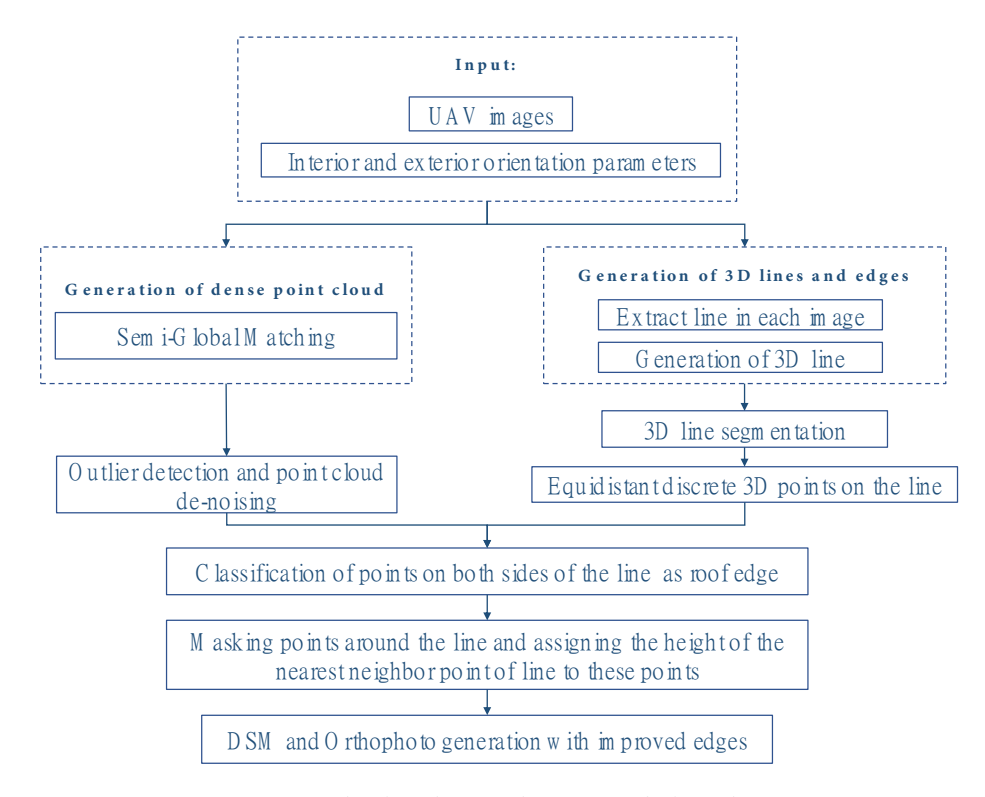


Figure 1. The flowchart of the proposed algorithm.

## 2.2.1. Generation of 3D dense point cloud

In digital photogrammetry, dense matching algorithms are used to generate dense point clouds. These methods automatically generate a dense point cloud by identifying common points in a stereo image pair. Once the parameters of exterior orientation and camera calibration are computed by aerial triangulation, a scene is reconstructed using SGM dense matching methods. At this step, millions of georeference points are generated. The dense point clouds generated in this way are then interpolated to produce a DSM (Linder, 2009).

Recently, Agisoft Metashape commercial software has been used to generate a dense point cloud in wide range of applications (Barbasiewicz et al., 2018). This software is a commercial package that can automatically orientate and match large unordered images. Due to the 3D results, the image matching algorithm implemented in this software is based on SGM (Deuber et al., 2014). This method provides a very good relationship between execution time and accuracy, especially at object boundaries and delicate structures. It is also resistant to radiometric differences and has less sensitivity to the choice of parameters; therefore, it is suitable for solving practical problems (Patil et al., 2019).

#### 2.2.2. Preprocessing

The point cloud is infected by some erroneous points that should be removed in advance to produce an accurate TIN model. Furthermore, the point cloud must be simplified to reduce the cost of computing and memory in producing the TIN model.

This step includes outlier detection and denoising to simplify the generated point cloud. Here, to detect the outliers, in addition to local density analysis in a neighbourhood radius, a local polynomial fitting method is used to eliminate the disadvantages of the global fitting method. In the local fitting method as a denoising step, the points that its z-component is far from the fitted local polynomial are eliminated (Deschaud & Goulette, 2010). To determine the neighbourhood for each point cloud data with x,y,z whose z component indicates on the point height data, the sphere equation from other points  $x_i, y_i, z_i$  is used as follows:

$$NPs = \sqrt{(x - x_i)^2 + (y - y_i)^2 + (z - z_i)^2}$$

$$< r \quad i = 1, 2, ..., N$$
(1)

In such a way that if the number of points inside the sphere with a certain radius (r) is less than a defined minimum number, that point is removed as an outlier. Using this algorithm, the point cloud that have a low density is removed. For the remaining points, a neighborhood is algorithmically defined to enable localized analysis.

After identifying the points that are in a neighborhood, an appropriate polynomial surface is fitted to the data with a proper degree depending on the type of data. Of course, there are some points that are not on the surface that can be removed using a certain threshold. For each x, y, a height

 $(z_p = f(x, y))$  is obtained through polynomials. For example, a polynomial of degree 2 is as follows:

$$f(x,y) = c_{00} + c_{10}x + c_{01}y + c_{20}x^2 + c_{11}xy + c_{02}y^2$$
(2)

By setting a threshold (t) for the difference in point height (z) from the height obtained from the polynomial  $(z_p)$ , points that are not placed on the surface with a large difference  $(z-z_p>t)$  can be treated through two strategies, 1) removing as a noisy point or 2) replacing its height with the height from the polynomial. Here, because the high density of points, the removing strategy is considered to simplify the point cloud. The optimal neighbourhood radius (r) and boundary thresholds (t) were empirically derived via systematic trial-and-error evaluation, assessing performance metrics surface smoothness.

## 2.2. Extraction of edge corners and 3D lines reconstruction

The production of 3D lines requires the accuracy of extracting 2D line features and edge corner. For this purpose, firstly the edge lines of the building are extracted using the Canny edge detector algorithm (Error! Reference source not found.-a). Then the corner points of the edges are extracted using the Harris corner detector algorithm (Error! Reference source not found.-b).

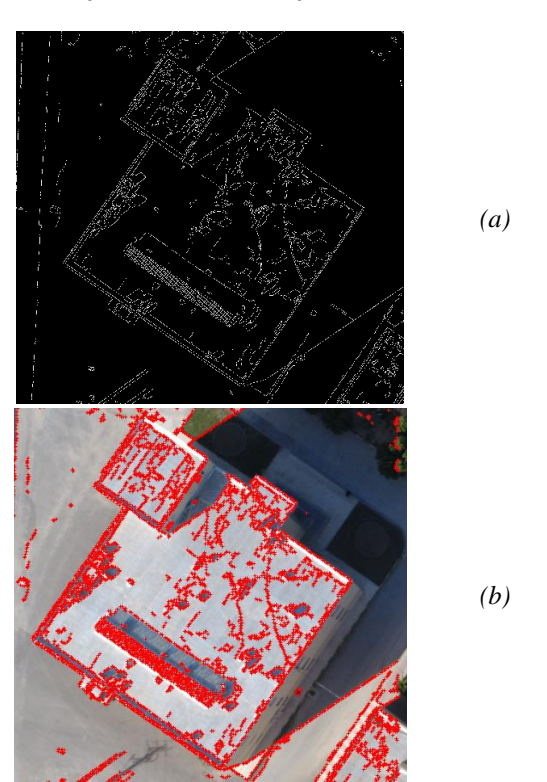


Figure 2. (a) Edges obtained by Canny (b) Corners obtained by Harris on sample image.

The edges of the building can be reconstructed by 3D lines. In this research, the 3D lines are generated using the multi-image bundle adjustment method. Since the current research is based on multi-images, the 3D line is extracted from the intersection of multi-plane planes, and since the intersection of the planes is not a single line, the optimum line is estimated from the intersection of planes in pairs based on the least squares method. These lines are divided into equidistant points and are integrated with the initial point cloud as additional points to model the edge of the building; therefore, 3D line production is done according to the following main processes:

- Reconstruction: 3D lines corresponding to the building edges are reconstructed without endpoints.
- Determination of the endpoints: Two ends of a 3D line are calculated by a rule-based method.
- Discretization: The 3D line is divided into equidistance 3D points.

# Step 1: Reconstruction of 3D line

In Figure 3, L is a 3D line that is reconstructed and estimated.  $O_1$  to  $O_n$  are the positions of the camera's perspective centres at the time of acquisition, and  $N_1$  to  $N_n$  are normal vectors on the planes  $P_1$  to  $P_n$ , respectively.

3D line equation corresponding to the edge of the building must first be calculated. The line equation that passes through the known point  $Q_0(x_0, y_0, z_0)$  and is parallel to the non-zero vector U = (p, q, r) known by parametric equation of line is as follows:

$$Q = Q_0 + t.U (t \in \mathbb{R}) (3)$$

Where U is the line direction vector and t is a scaler. The direction vector obtained from the intersection of two planes is easily obtained by using the external multiplication of normal vectors on the planes. The normal vector on a plane is obtained by using the external multiplication between the direction vectors of the OB line and the OE line passing through each P plane (Error! Reference source not found.). To calculate line direction vectors, two points on the line must be known. To obtain these points, the ground coordinates of the endpoints of line l are calculated. The inverse of the collinearity condition is used to calculate these points as follows:

$$[X_B - X_0 \quad Y_B - Y_0 \quad Z_B - Z_0]^T$$

$$= \lambda R[x_b \quad y_b - f]^T$$
(4)

Where  $(X_0, Y_0, Z_0)$  are the perspective centre of the image,  $(X_B, Y_B, Z_B)$  are the ground coordinates of point B and  $(x_b, y_b)$  are the image coordinates of point B, and f is the focal length of the camera. R is the rotation matrix around the coordinate axes, which is obtained as follows:

$$R = R_K R_{\omega} R_{\omega} \tag{5}$$

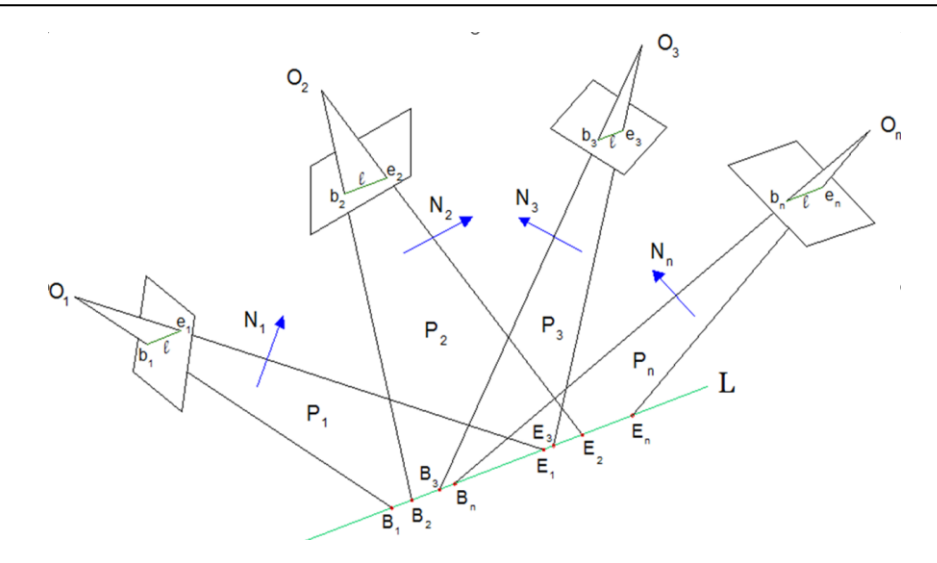


Figure 3. Reconstruct the three-dimensional line L with the intersection of n planes of n images.

 $R_{\omega}$ ,  $R_{\varphi}$  and  $R_K$  are rotation matrix around the X, Y and Z axis respectively. The parameter  $\lambda$  is a scale factor used to determine the exact location of a point. More than one image is needed to obtain the  $\lambda$  parameter. This section does not require the exact ground coordinates of point B, and to find the direction vector of the line, it is sufficient to obtain the direction of the line OB, therefore the parameter  $\lambda$  in the relations is omitted; the direction vector of the OB line is calculated as follows:

$$H_{OB} = (X_B - X_O, Y_B - Y_O, Z_B - Z_O)$$
 (6)

In the same way, the direction vector of the OE line is obtained. Next, the normal vector of the P plane is calculated as follows:

$$N = H_{OB} \times H_{OE} = (a b c) \tag{7}$$

Note that the normal vector of the plane must be normalized using  $Nn = N/\sqrt{(\sum N_{ij}^2)}$ . Therefore, in this study, N means  $N_n$ . In case of extraction of optimum line from multi-images to get the 3D line direction vector, if all the planes in a line intersect, U can be calculated exactly for this line. But if they are not in a line intersecting, but in pairs intersecting in a line, the least squares method is used to find the optimum U. Since  $U.N_j = 0$  applies to each plane number j, which U is simply calculated by  $U = N_1 \times N_2$ , the system of least squares prepared as follows:

$$\min_{U} ||N.U|| \tag{8}$$

If the planes do not intersect, the above relation is equal to zero. A simple way is to calculate the mean of  $N_i \times N_j$ , which is the direction vector of the intersection line for both planes, and the mean of this set is chosen as U. Another way is to try for minimization as follows:

$$\min_{U} \sum_{i,j} \left\| U - N_i \times N_j \right\|^2 \tag{9}$$

So that the obtained U, is the closest parallel line to the direction vector of the line from the intersection of both planes means the least squares. In this minimization it is necessary that all normal vectors on the planes are in the same direction, i.e.,  $(N_i \times N_j).(N_k \times N_l) \ge 0$ , because  $N_i \times N_j = -N_j \times N_i$ . The final minimization is the mean of the  $(N_i \times N_j)$ .

Then a fixed 3D point  $Q_0$  through which line L passes is computed. This point must minimize the orthogonal distance to all planes. The system of equations for determining  $Q_0$  is formulated as follows:

$$dist(Q_0, P_k) = |N_k, (Q_0 - Q_k)| \to min \tag{10}$$

Where the  $P_k$  represents the  $k^{th}$  plane  $N_k$  is the normal vector to the  $k^{th}$  plane, and  $Q_k$  denotes an arbitrary point on the  $k^{th}$  plane. In this study, the perspective centres of the images are used as  $Q_k$ . This relation is expressed in matrix form as follows

$$NQ_{0} = \begin{bmatrix} N_{1,1} & N_{1,2} & N_{1,3} \\ N_{2,1} & N_{2,2} & N_{2,3} \\ \vdots & \vdots & \vdots \\ N_{m,1} & N_{m,2} & N_{m,3} \end{bmatrix} \cdot \begin{bmatrix} X_{Q_{0}} \\ Y_{Q_{0}} \\ Z_{Q_{0}} \end{bmatrix}$$
(11)

$$A = N_{k}Q_{k} = \begin{bmatrix} N_{1} & Q_{1} \\ N_{2} & Q_{2} \\ \vdots \\ N_{m} & Q_{m} \end{bmatrix}$$
(12)

Where the matrix N is a  $m \times 3$  matrix which is a list of normal vectors in rows. The least squares formulation for eq. (12) is as follows:

$$\min_{Q_0} ||NQ_0 - A|| \tag{13}$$

Therefore, the point  $Q_0$  is obtained as follows:

$$NQ_0 = A \implies N^T N Q_0 = N^T A \implies$$

$$Q_0 = (N^T N)^{-1} N^T A$$
(14)

Now, by specifying the direction vector of the 3D line L and the fixed point  $Q_0$  on that line, the line equation can be formed according to eq. (3).

Step 2: Determination of the endpoints of the 3D line

The lines reconstructed by the intersection of several plane in the last step are infinite lines whose endpoint coordinates are not known. To integrate the segments of the line L to the initial point cloud, the endpoints of the line need to be determined; therefore, the edge lines of the building must be finite and contain two endpoints. Next, the positions of the endpoints of the 3D line are calculated based on the "longest length rule". The longest length rule refers to a heuristic where the longest continuous edge or contour within a segmented region is prioritized for further analysis.

As shown in Error! Reference source not found., the coordinates of points B and E corresponding to the endpoints of line L can be calculated using the coordinates b and e corresponding to the endpoints of line l in each image. According to the longest length rule, the endpoints of the 3D line L are  $B_1E_n$ . In eq. (3), any point on a 3D line can be represented by a different scale factor. For the end points of each line in each image, two factors so, for n aerial scenes, 2n scale factors are calculated. According to eq. (3) it can be written:

$$Q - O = Q_0 + t \cdot U - O (15)$$

Where  $Q - O = [X - X_0 \ Y - Y_0 \ Z - Z_0]^T$ . So, eq. (4) is placed in eq. (15):

$$\lambda R[x_b \ y_b - f]^T = Q_0 - O + t.U \Rightarrow$$

$$\begin{bmatrix} -U & R[x_b & y_b - f]^T \end{bmatrix} \begin{bmatrix} t \\ \lambda \end{bmatrix} = Q_0 - O$$
 (16)

If  $A = \begin{bmatrix} -U & R[x_b & y_b - f]^T \end{bmatrix}$  and  $Q_0 - O = b$ , t and  $\lambda$  are calculated using the least squares approach as follows:

Similarly, the scale factor of line endpoints in all images is calculated using eq. (17). Finally, the endpoints of the 3D line are calculated by substituting the values of  $t_{min}$  and  $t_{max}$  for scale factor in the 3D line equation.

Step 3: Discretization of the 3D line

3D line segments cannot be integrated into the initial point cloud due to the linear nature, so it is necessary to divide the 3D line segments into equidistant 3D points. If the number of discrete points from the 3D line is considered m, the distance between the two discrete points is calculated from the following equation:

$$\Delta t = (t_{\text{max}} - t_{\text{min}})/_{m} \tag{18}$$

where m is obtained based on the density of the point cloud through trial and error.

The coordinates of discrete 3D points are obtained from the following equation:

$$Q_{i} = Q_{0} + (t_{min} + i * \Delta t) * U$$

$$(i = 1, 2, ..., m)$$
(19)

The obtained points are integrated to the initial 3D point cloud as additional points to improve the DSM.

## 2.3. Refinement of edge point clouds to Improve DSM

Step 1: Classification of points on both sides of the building edge

At this step, the edge line is considered as a border, and points are classified based on which side of the edge they are located on. In this way, two classes of points one on the roof and the other on the ground, are formed.

For this process, first, regardless of the z component, a 2D line is fitted to the set of edge points and the vertical distance of the points to the line is calculated, based on the 2D general line formula (ax + by + c = 0), that its equation is as follows:

$$d = \frac{ax_0 + by_0 + c}{\sqrt{a^2 + b^2}}$$

(20)

Then, points with positive or negative distance are placed in two different classes, which are referred to as on the roof and on the ground class according to the position of the points.

Step 2: Masking points around the line between the inner and outer edges as the parapet wall of the roof, and the average height of the points inside the mask is assigned to all masked point clouds. In this step, according to the vertical distances calculated by eq. (20) from the inner and outer edge line, the points whose vertical distance from the two lines ( $d_1$  and  $d_2$ ) have opposite signs or in other words, according to Figure 4., ( $d_1.d_2<0$ ) are placed between the two lines.

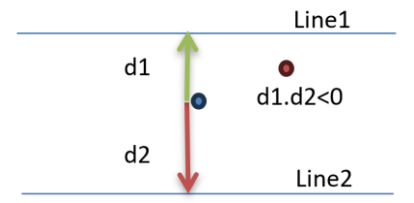


Figure 4. Schematic representation of the distance from two lines for points between them.

Therefore, a mask with a small width (the approximate thickness of the parapet wall) is formed around the line, and among the points of the roof class, those that are inside this mask are separated and instead of the observed height, the average height of the points inside the mask is assigned to all masked point clouds. Also, the developed discrete points of both lines according to section 2.2 are added to the point clouds of the roof. In this way, the points on the roof edge are placed more sharply among other points.

## Step 3: Improved DSM and orthophoto generation

By integration of point clouds by refined edge points, an accurate elevation model as well as an improved DSM are

produced. Triangulated irregular network (TIN) is used as an interpolation method to produce a DSM. Furthermore, the improved point cloud according to the edge of the building are introduced to generate orthophoto.

# 3. Experimental Results and Discussion

To evaluate the efficiency of the proposed method in improving DSM and orthophoto and multiple UAV images are used (Error! Reference source not found.).



Figure 5. Four UAV images in the study area.

Implementation of the proposed method is performed in MATLAB 2019 and Agisoft commercial software. In order to analyze the efficiency of the proposed method, a building edge is chosen in four overlapping images, and further results are shown on this edge. The proposed method contains two parameters (r and t as presented in section 2.1.2), which should be set before implementation. The optimum values for these parameters are defined by trial and error. The radius and threshold are set to 0.2 and 0.02 meter, respectively.

Firstly, aerial triangulation is performed and photogrammetric productions (point cloud, TIN model, DSM, and ortho-mosaic) are generated in a common photogrammetry process. Error! Reference source not found. demonstrates TIN model building.

As shows **Error! Reference source not found.** that, TIN model contains several heterogeneous elements in the building wall and distortions in building edges.

Error! Reference source not found. illustrates the initial building which is generated in the standard

photogrammetric process. Two building edges are shown in a closer look.

DSM analysis depicts that there are some planimetric and altimetric variations in building edges. These challenges lead to saw-tooth effect in orthophoto. The mono-plotting process presents significant challenges in implementation. **Error! Reference source not found.** displays the derived orthophoto generated from the initial DSM, achieving a spatial resolution of 3 cm.

In the next step, 3D lines corresponding to the edges are generated and added to the initial point cloud. The production of 3D lines requires the accuracy and precision of extracting lines and 2D edge corners in image. After obtaining the corner points of the building edge these points are used to produce 3D lines. In the proposed method, these lines are divided into discrete points with a certain density (Error! Reference source not found.).

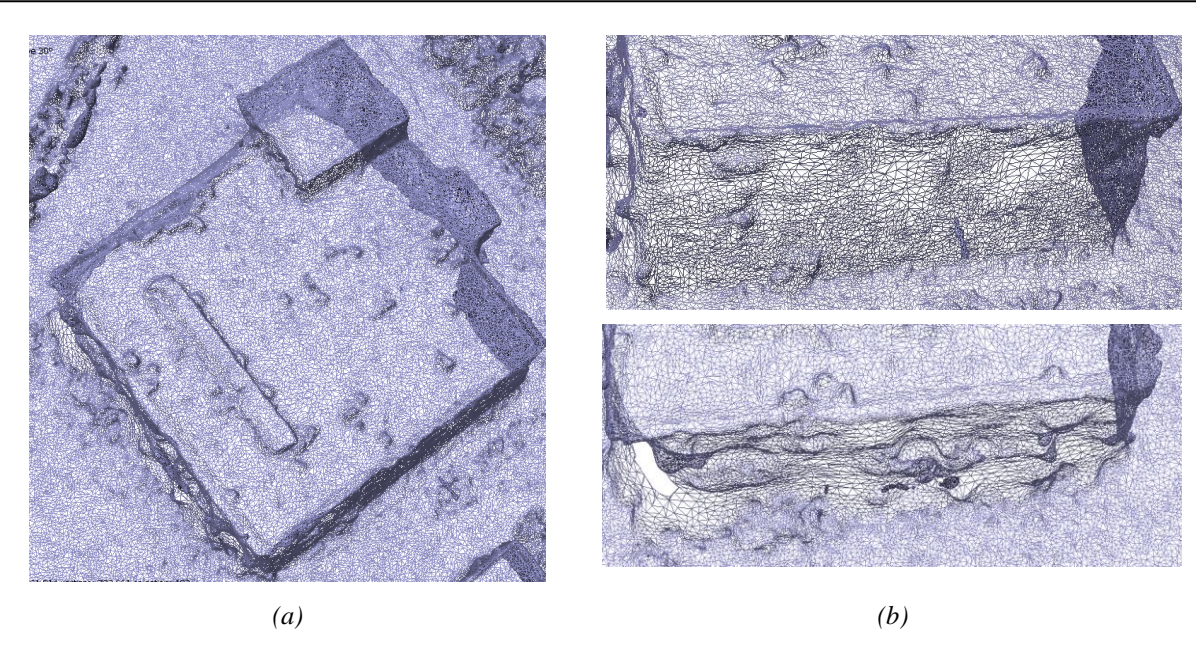


Figure 6. (a) TIN model (b) TIN around edges for the first building.

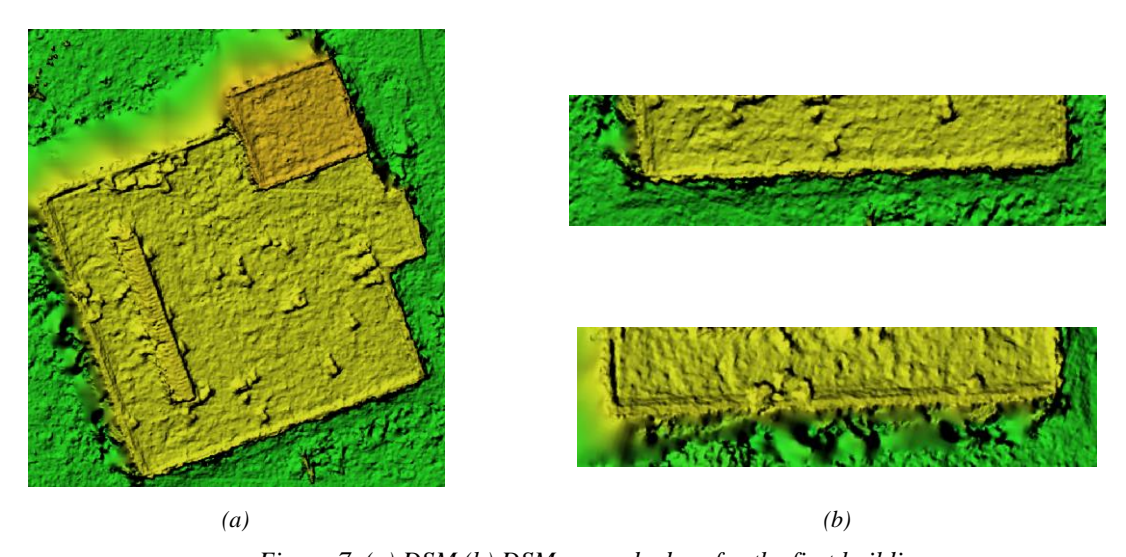


Figure 7. (a) DSM (b) DSM around edges for the first building.



Figure 8. Orthophoto for the first building outlines based on the initial DSM

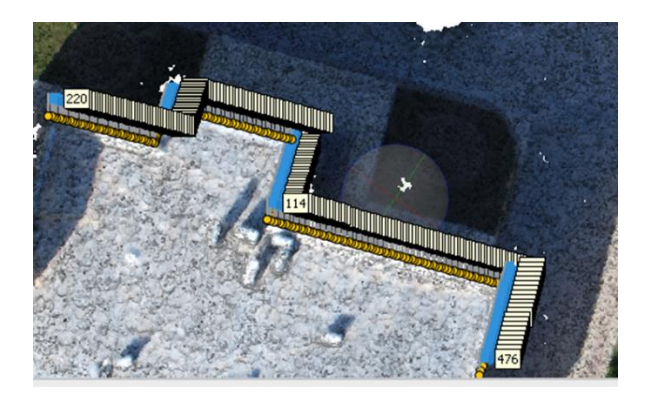


Figure 9. 3D points produced by the proposed method with a density of 17 cm.

The obtained 3D point cloud is classified on both sides of the line and the points around the line are masked; then the average height of the points inside the mask is assigned to all masked point clouds. By integration of points of 3D line into the initial point cloud to create a modified TIN (Error! Reference source not found.).

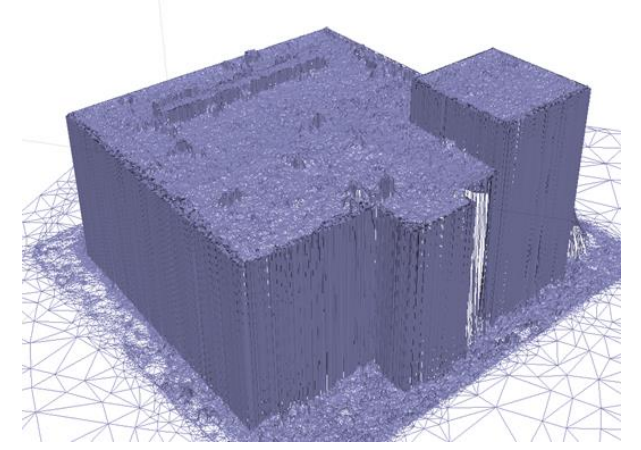


Figure 10. (a) TIN model of the first building in the modified point cloud.

Comparing Error! Reference source not found. and Error! Reference source not found. proves the ability of the proposed method in TIN generation. The modified model reaches better quality in the wall where discontinuity is preserved. For better analysis, DSM is generated based on new point cloud which is shown in Error! Reference source not found..

Comparative analysis reveals a significant enhancement in building edge delineation in both TIN and DSM models. The sharp building boundaries observed in the DSM results validate the superior performance of the proposed approach. Finally, the improved orthophoto is derived based on a modified DSM. Error! Reference source not found. depicts the obtained orthophoto in building boundaries.

Comparison of modified ortho (Error! Reference source not found.) with initial orthophoto (Error! Reference source not found.) proves that saw-tooth effects have improved on the edges of the building in the generated orthophoto based on the modified point cloud. In order to prove the high potential of the proposed method, another building is considered. Error! Reference source not found. shows the effects of the proposed method on the generated TIN.

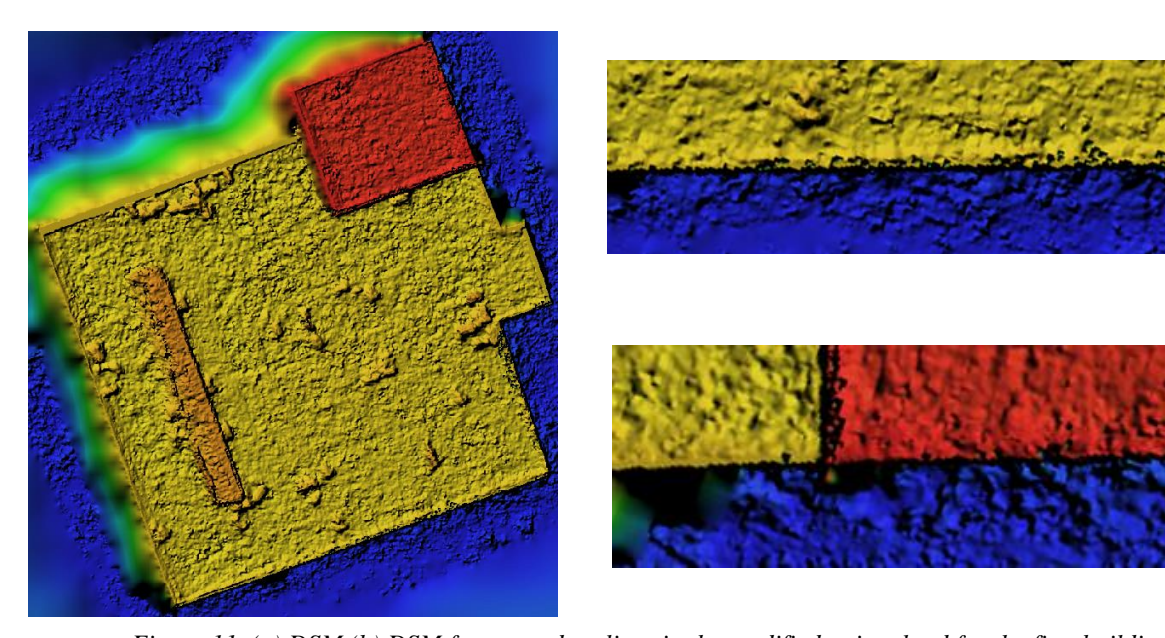


Figure 11. (a) DSM (b) DSM for around outlines in the modified point cloud for the first building.

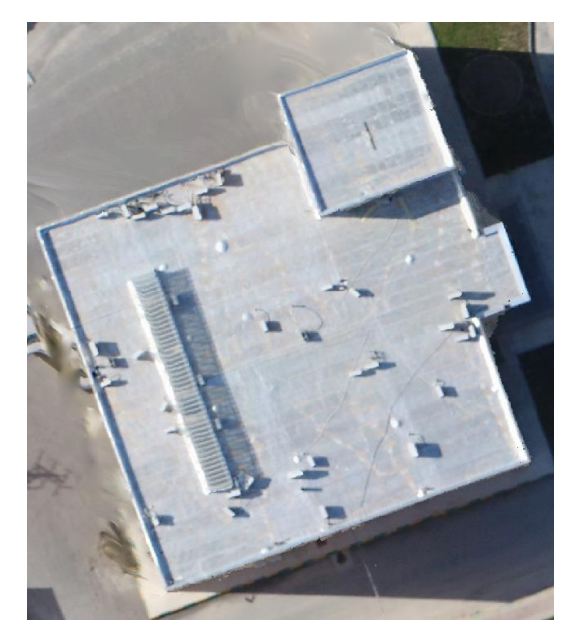
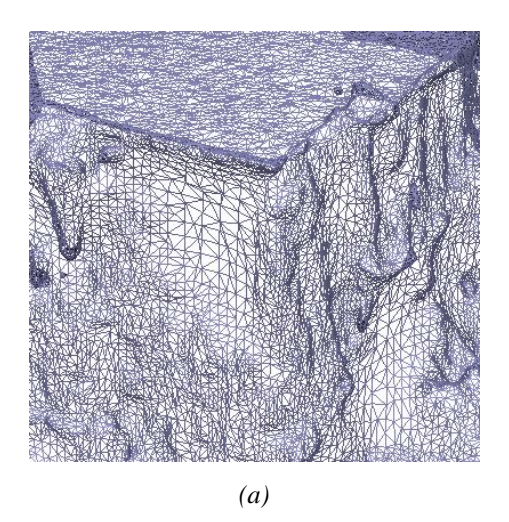






Figure 12. (a) Orthophoto (b) Orthophoto around outlines based on the modified DSM for the first building.



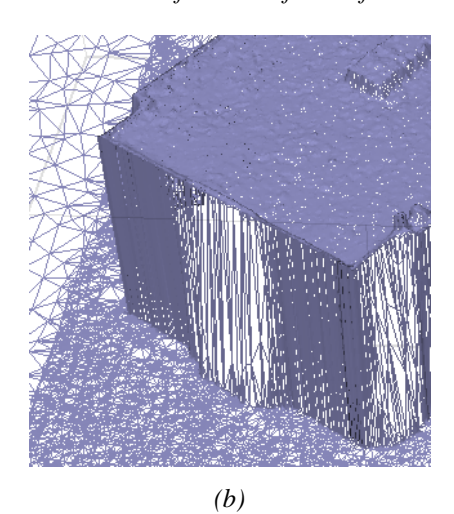
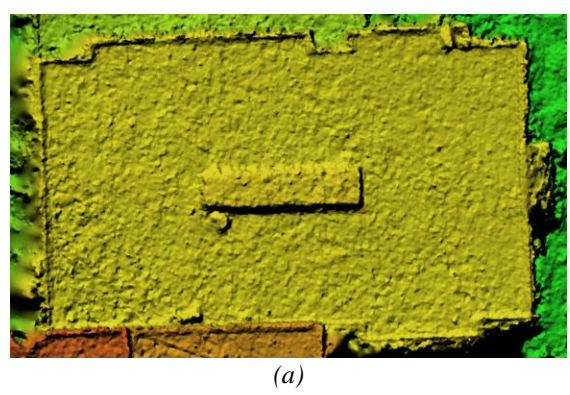


Figure 13. TIN based on (a) initial point cloud (b) improved point cloud for the second building.

Analyzing the above figure shows that the proposed method significantly improves the TIN quality. It contains homogenous triangles and also discontinuities are preserved. In order to evaluate the height information around building edges, DSM is generated based on initial and improved point cloud (Figure 14).

Comparing two DSMs depicts that the improved point cloud and also the preprocessing steps made building edges better. Finally, Orthophoto is generated based on the improved DSM. Figure 15 illustrates the orthophoto around the second building, which are generated based on the initial DSM and improved one.



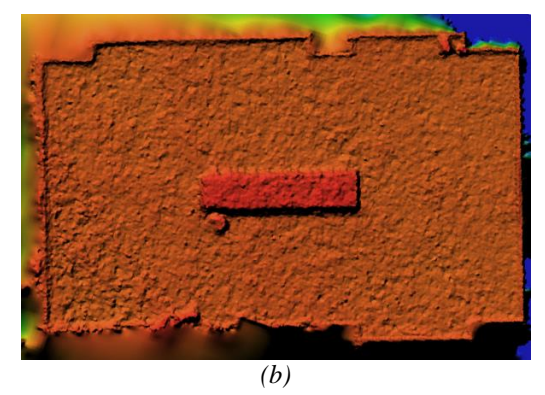
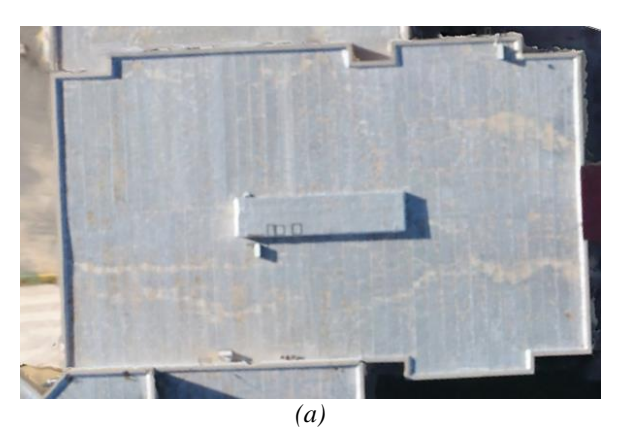


Figure 14. DSM based on (a) initial point cloud (b) improved point cloud for the second building.



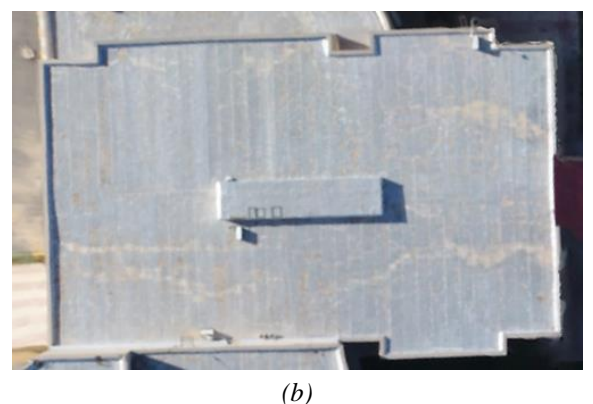


Figure 15. Orthophoto based on (a) initial DSM (b) improved DSM for the second building.

As Error! Reference source not found. shows, saw-tooth effects and distortion near building edges have decreased significantly, which proves the high potentiality of the proposed method. For the statistical evaluation of the modified point clouds by an edge line, a band with a certain width is created around the line. The mask width is empirically determined as a function of wall thickness, typically ranging between 20-30 cm for standard urban building parapets. Then the height difference of the points inside the band compared to the nearest points on the line before and after implementation of that as the edge of the building is calculated and then the statistical parameters of this difference vector is calculated. For this purpose, three lines are considered as shown in Error! Reference source not found.

The statistical parameters of the height differences of the points around the edge (the band widths of 20 cm) before and after adding the line 1 are presented in Table 1, as well as the histogram of the height of the points inside the band, are presented in **Error! Reference source not found.**.

The statistical parameters of the height differences of the points around the edge (the band widths of 20 cm) before and after adding the line 2 are presented in Table 2, as well as the histogram of the height of the points inside the band, are presented in **Error! Reference source not found.**.



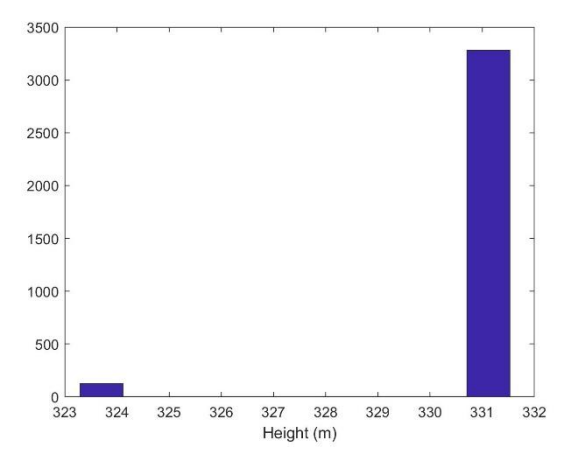
Figure 16. Three considered lines.

The statistical parameters of the height differences of the points around the edge (the band widths of 20 cm) before and after adding the line 3 are presented in Table 3, as well as the histogram of the height of the points inside the band, are presented in **Error! Reference source not found.** 

The statistical results in all three above cases show a decrease in the height distribution of the points around the edge line after implementation of the line in the point clouds. The reduction of the height distribution of the points around the edge and its proximity to the height of the line points had a great impact on the results of the TIN and the DEM, and its effect can be seen in the orthophoto results.

Table 1. The statistical parameters of the height differences of the points in a buffer with a width of 20 cm, before and after adding the line 1 (in meters).

		Min	Max	Mean	STD	RMS	
	Before the line adding	0	8.0161	-0.4672	1.4395	1.5132	
	After the line adding	0	0.4366	-0.0972	0.1269	0.1599	



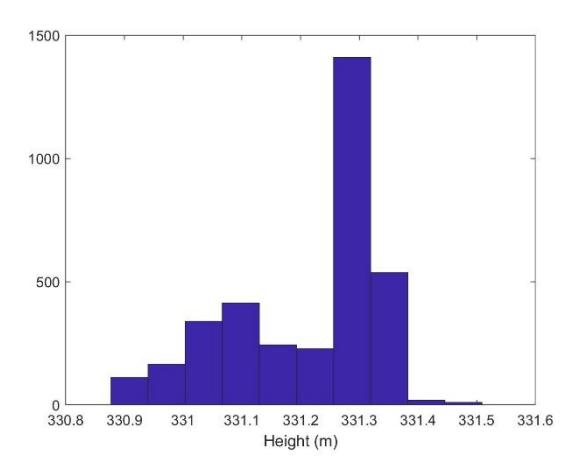
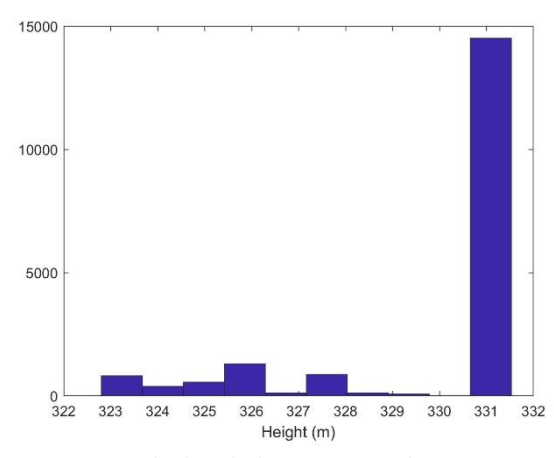


Figure 17. The height histogram of the points in a buffer with a width of 20 cm, before and after the addition of line 1.

Table 2. The statistical parameters of the height differences of the points in a buffer with a width of 20 cm, before and after adding the line 2 (in meters).

	Min	Max	Mean	STD	RMS	
Before the line adding	0	8.4721	-1.4519	2.3936	2.7995	
After the line adding	0	6.1832	-0.1486	0.5430	0.5630	



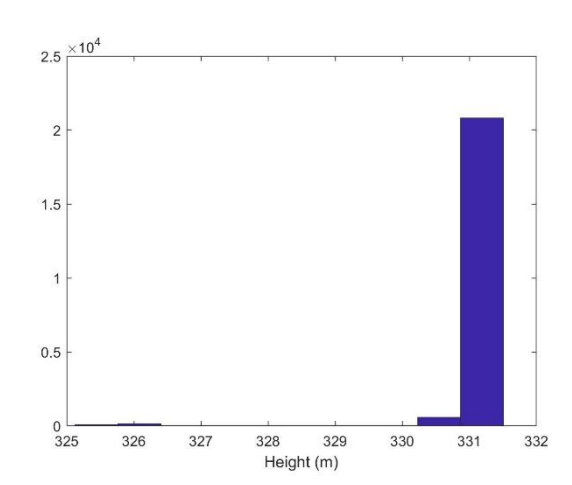
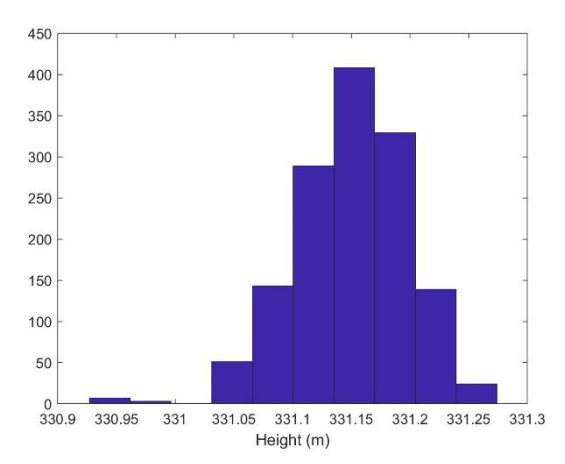


Figure 18. The height histogram of the points in a buffer with a width of 20 cm, before and after adding line 2.

Table 3. The statistical parameters of the height differences of the points in a buffer with a width of 20 cm, before and after adding the line 3 (in meters).

	Min	Max	Mean	STD	RMS
Before the line adding	0.0001	0.2982	-0.0787	0.0487	0.0925
After the line adding	0	0.1920	-0.0143	0.0413	0.04367



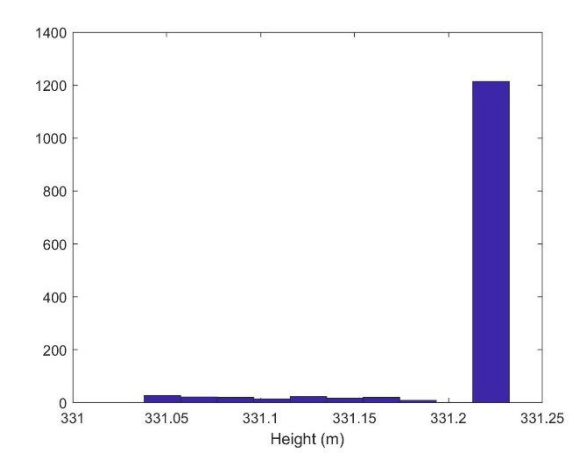


Figure 19. The height histogram of the points in a buffer with a width of 20 cm, before and after adding line 3.

Since the average height of the points inside the mask is assigned to all masked point clouds, the height variation among masked points becomes significantly reduced. Consequently, it is logically expected that the maximum and minimum height differences within this region diminish substantially. Regarding the STD and RMS, the height dispersion of points within the mask has improved by up to 99% in maximum achievable performance. Furthermore, the height histogram demonstrates a significant reduction in dispersion. The 99% reduction in height variance (STD) minimizes erratic height jumps. Precise parapet wall thickness-based masking preserves true roof boundaries while filtering outliers.

# 4. Conclusion

This research has presented a new approach for reconstructing DSM by extracting parts of 2D building edges from UAV multi-images. In the first step, after generating the initial point cloud, 2D line segments are extracted, then 3D lines are generated from the intersection of two-dimensional lines using the bundle adjustment method. For this purpose, multi-planes are intersected and best 3D line is generated least square. The two endpoints of the 3D line are estimated by calculating the longest length using four image points. Finally, the 3D line segments defined by the two endpoints are discretised and integrated with the initial point cloud for reconstruction of the TIN and DSM model besides the orthophoto production. Both visual and numerical evaluations of the building image dataset demonstrate that the proposed method effectively reduces saw-tooth artifacts in the orthophoto while substantially improving DSM quality. Although, the proposed method reaches the high accuracy and good interpretation results, it has some limitations, such as occlusion in oblique images and proximity to other objects (e.g. trees) in complex urban areas. For future work, we suggest evaluating the proposed method on the diverse building types in different areas.

Moreover, the sensitivity analysis of the proposed method to its parameters is suggested.

# Data Availability

Data is not available.

#### References

Alidoost, F., Arefi, H., & Tombari, F. (2019). 2D image-to-3D model: Knowledge-based 3D building reconstruction (3DBR) using single aerial images and convolutional neural networks (CNNs). Remote Sensing, 11(19), 2219. https://doi.org/10.3390/rs11192219

Barbasiewicz, A., Widerski, T., & Daliga, K. (2018). The analysis of the accuracy of spatial models using photogrammetric software: Agisoft Photoscan and Pix4D. E3S Web of Conferences. https://doi.org/10.1051/e3sconf/20182600012

Bhandari, B., Oli, U., Pudasaini, U., & Panta, N. (2015). Generation of high resolution DSM using UAV images. FIG working week,

Bignoli, A., Romanoni, A., Matteucci, M., & di Milano, P. (2018). Multi-view stereo 3D edge reconstruction. 2018 IEEE Winter Conference on Applications of Computer Vision (WACV), https://doi.org/10.1109/WACV.2018.00100

Chen, Q., Zhang, Y., Li, X., & Tao, P. (2021). Extracting Rectified Building Footprints from Traditional Orthophotos: A New Workflow. Sensors, 22(1), https://doi.org/207. 10.1109/WACV.2018.00100

Chuang, T.-Y., Ting, H.-W., & Jaw, J.-J. (2018). Dense stereo matching with edge-constrained penalty tuning. IEEE Geoscience and Remote Sensing Letters, 15(5), https://doi.org/664-668. 10.1109/LGRS.2018.2805916

Dall'Asta, E., & Roncella, R. (2014). A comparison of semiglobal and local dense matching algorithms for surface reconstruction. The international

- archives of the photogrammetry, remote sensing and spatial information sciences, 40, 187-194. https://doi.org/10.5194/isprsarchives-XL-5-187-2014
- Deschaud, J.-E., & Goulette, F. (2010). Point cloud non local denoising using local surface descriptor similarity. PCV (Photogrammetric Computer Vision).
- Deuber, M., Cavegn, S., & Nebiker, S. Dense Image Matching.
- Ebrahimikia, M., & Hosseininaveh, A. (2022). True orthophoto generation based on unmanned aerial vehicle images using reconstructed edge points. The Photogrammetric Record, 37(178), 161-184. https://doi.org/10.1111/phor.12409
- Jiménez-Jiménez, S. I., Ojeda-Bustamante, W., Marcial-Pablo, M. d. J., & Enciso, J. (2021). Digital terrain models generated with low-cost UAV photogrammetry: Methodology and accuracy. ISPRS International Journal of Geo-Information, 10(5), 285. https://doi.org/10.3390/ijgi10050285
- Linder, W. (2009). Digital photogrammetry (Vol. 1). Springer.
- Liu, J., Gao, J., Ji, S., Zeng, C., Zhang, S., & Gong, J. (2023). Deep learning based multi-view stereo matching and 3D scene reconstruction from oblique aerial images. ISPRS Journal of Photogrammetry and Remote Sensing, 204, 42-60. https://doi.org/10.1016/j.isprsjprs.2023.08.01 5
  - Liu, J., Wang, H., Liu, X., Li, F., Sun, G., & Song, P. (2015). An automated 3D reconstruction method of UAV images. AOPC 2015: Telescope and Space Optical Instrumentation, https://doi.org/10.1117/12.2199631
- Lu, Z., Wang, J., Li, Z., Chen, S., & Wu, F. (2021). A resource-efficient pipelined architecture for real-time semi-global stereo matching. IEEE Transactions on Circuits and Systems for Video Technology, 32(2), 660-673. https://doi.org/10.1109/TCSVT.2021.3061704
- Ma, Y., Fang, X., Dong, P., Guan, X., Li, K., Chen, L., & An, F. (2022). Subpixel Interpolation Disparity Refinement for Semi-Global Matching. 2022 IEEE Asia Pacific Conference on Circuits and Systems (APCCAS), https://doi.org/10.1109/APCCAS55924.2022.1
- McIntosh, K., & Krupnik, A. (2002). Integration of laserderived DSMs and matched image edges for generating an accurate surface model. ISPRS Journal of photogrammetry and Remote Sensing, 56(3), 167-176. https://doi.org/10.1016/S0924-2716(02)00042-4

0090384

- Nex, F., & Remondino, F. (2014). UAV for 3D mapping applications: a review. Applied geomatics, 6, 1-15. https://doi.org/10.1007/s12518-013-0120-x
- Patil, S., Prakash, T., Comandur, B., & Kak, A. (2019). A comparative evaluation of SGM variants (including a new variant, tMGM) for dense stereo matching. arXiv preprint arXiv:1911.09800. https://doi.org/10.48550/arXiv.1911.09800
- Qin, R., Gruen, A., & Fraser, C. (2021). Quality assessment of image matchers for DSM generation--a comparative study based on UAV images. https://doi.org/10.13140/2.1.3108.0005
- Shao, Z., Yang, N., Xiao, X., Zhang, L., & Peng, Z. (2016).

  A multi-view dense point cloud generation algorithm based on low-altitude remote sensing images. Remote Sensing, 8(5), 381. https://doi.org/10.3390/rs8050381
- Su, N., Yan, Y., Qiu, M., Zhao, C., & Wang, L. (2018).

  Object-based dense matching method for maintaining structure characteristics of linear buildings. Sensors, 18(4),

  https://doi.org/10.3390/s18041035
- Wang, Q., Yan, L., Sun, Y., Cui, X., Mortimer, H., & Li, Y. (2018). True orthophoto generation using line segment matches. The Photogrammetric Record, 33(161), 113-130. https://doi.org/10.1111/phor.12229
- Wu, B. (2021). Photogrammetry for 3D mapping in Urban Areas. Urban informatics, 401-413. https://doi.org/10.1007/978-981-15-8983-6 23
- Yue, X., Wang, F., Guo, B., Xu, P., & Shi, J. (2018).

  Disparity map optimization based on edge detection. Chinese Control And Decision Conference (CCDC), Shenyang, China, 2018, pp. 3311-3315.
  - https://doi.org/10.1109/CCDC.2018.8407696.